DOI: 10.1002/anie.201104270

Lithography

Patterning Materials through Viscoelastic Flow and Phase Separation**

*Minwoo Park, Younan Xia, and Unyong Jeong**

Many non-photolithographic techniques have been developed for large-area patterning, with soft lithography being the most successful example. In the form of microcontact printing,[1] nanoimprinting,[2] capillary force lithography,[3] or replica molding,[4] soft lithography uses an elastomeric mold bearing a patterned surface to generate or transfer submicrometer-sized structures without the need to access complicated and often expensive apparatus. In spite of its great potential as a versatile approach to the fabrication of structures down to less than 100 nm, the materials that can be easily and directly patterned using soft lithography are still limited to self-assembled monolayers, polymers, and sol-gel materials.[5,6] Even though several have employed soft lithography to pattern organic/inorganic hybrid materials[7,8] or have used a polymer pattern as a sacrificial template for patterning inorganic materials,[9,10] fine structures of inorganic materials are fabricated by conventional photolithography in combination with vacuum deposition.[11,12]

Here we report a simple and versatile method for patterning inorganic materials. Figure 1 shows the fabrication process. The material to be patterned was randomly deposited on the surface of a substrate that had been patterned with a polymer using capillary force lithography (CFL). The criteria for selecting a polymer were cheap and fast processes, low processing temperatures, and applicability to diverse materials. Specific consideration was placed on water- or alcohol-dispersible materials to follow the current trend in practical uses. A crystalline polymer is advantageous for this process because an abrupt drop in viscosity at the melting temperature (T_m) can facilitate the formation of a polymer pattern without a residual layer.[13] A hydrophobic polymer is appropriate to induce phase separation between the polymer and the hydrophilic materials. Thereby, hydrophobic crystalline polymers with a low melting temperature (but higher than room temperature) were selected. Here we used poly(ε-caprolactone) (PCL, $T_m = 60\,°C$) to prove the concept. When heated above the T_m of the polymers, the viscoelastic polymer liquid spreads to the recessed area and covers the entire surface of a substrate. If a material placed on the polymer pattern is incompatible to the polymer, it will be phase-separated and pushed by the polymer flow towards the center of the recessed region. The polymer melt will keep the material in the recessed region until it evolves into a continuous feature. Hard materials with a melting point higher than the annealing temperature tend to sink down to the substrate and the polymer liquid evolves into a thin film with a smooth surface. In contrast, soft materials with a melting point lower or comparable to the annealing temperature are transformed into the liquid phase during heating, then evolve into structures with a sharp interface to the polymer liquid. Amorphous polymers are not appropriate for this purpose because of their high viscosity and slow fluidic velocity (see the Experimental Section, Table S1, and Figure S1 in the Supporting Information).

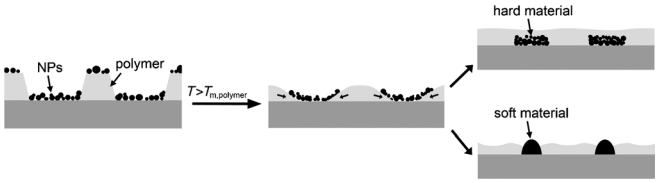

Figure 1. Self-organization of nanoparticles (NPs) scattered on a polymer pattern. When heated above the melting temperature (T_m), the polymer flows down to the recessed regions of a pattern, pushing the nanoparticles to the center of each recessed region. Hard materials with melting points higher than the annealing temperature sink down to the substrate and evolve into continuous, porous lines. Soft materials form a sharp interface with the polymer liquid and evolve into porous, solid lines.

Figure 2 a–f shows the patterning of Ag as an example of hard materials. In this case, a solution of $AgNO_3$ in ethanol was spread on the surface of a PCL pattern on a Si wafer. The surface of the PCL pattern had been treated with oxygen plasma. The Ag precursor was then reduced into Ag nanoparticles (30–50 nm in size) by exposure to N_2H_4 vapor. Figure 2 a,b shows atomic force microscopy (AFM) images of the sample in the height and phase modes, respectively. Figure 2 c shows a scanning probe microscopy (SEM) image of the same sample, which shows the Ag nanoparticles everywhere on the surface. Figure 2 d–f displays the organization of the Ag nanoparticles after the sample had been annealed at 150 °C for 30 s. The AFM image in Figure 2 d

[*] M. Park, Prof. Y. Xia, Prof. U. Jeong
Department of Materials Science and Engineering
Yonsei University, 134 Shinchon-dong, Seoul (Korea)
E-mail: ujeong@yonsei.ac.kr
Prof. Y. Xia
Department of Biomedical Engineering
Washington University in St. Louis
1 Brookings Drive, St. Louis, MO63130 (USA)

[**] This research was partly supported by the National Research Foundation (NRF) grant funded by the Korean Government (MEST) through the Active Polymer Center Pattern Integration (No. R11-2007-050-01004-0), the World Class University Program (R32-20031), and the Fusion Research Program for Green Technologies (2011-0000004).

Supporting information for this article including experimental details, microscopy analysis of the patterns, and kinetic experimental results is available on the WWW under http://dx.doi.org/10.1002/anie.201104270.

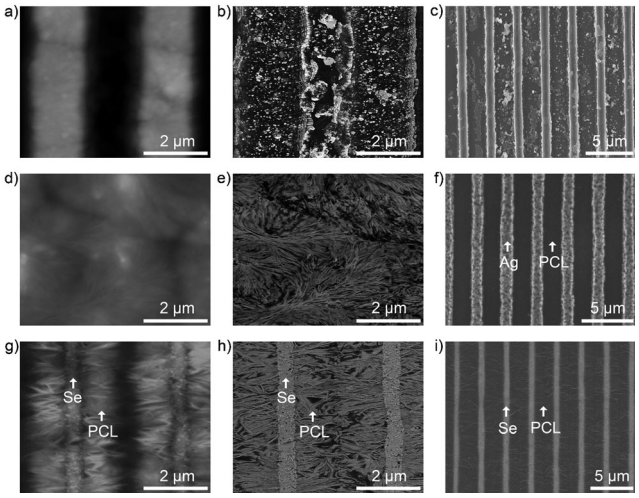

Figure 2. AFM images in the a) height and b) phase modes, and a SEM image of c) Ag nanoparticles (30–50 nm) scattered on a pattern of PCL lines. d–f) Porous lines of Ag generated from Ag nanoparticles scattered on the PCL pattern. The Ag nanoparticles were covered by the polymer as observed in the AFM images recorded in the d) height and e) phase modes. The backscattered SEM image in (f) indicates that the particles were concentrated in the center of the recessed area. AFM images in the g) height and h) phase modes, and a SEM image of i) continuous Se lines obtained from the Se nanoparticles scattered on the same PCL pattern.

indicates that the polymer structures had been transformed into a flat film with a smooth surface. Polymer crystal spherulites were observed on the entire surface (Figure 2e), suggesting that the Ag nanoparticles were positioned below the polymer layer. Figure 2f shows a backscattered SEM image, revealing that the Ag nanoparticles had assembled into solid lines in the recessed regions. The Ag nanoparticles could readily sinter into continuous lines at the annealing temperature because their surface was not passivated by any surfactant. The kinetic variables in the process include the annealing temperature, annealing time, thickness of the residual polymer layer, and coverage of the nanoparticles. We investigated the effect of the experimental variables (see the Experimental Section and Figures S2 and S3 in the Supporting Information). Long-time annealing and the thickness of the residual polymer layer in the polymer pattern did not make any difference in the morphology. Using a large number of nanoparticles led to thicker rather than wider lines. Direct annealing at high temperatures (> 180 °C) caused large droplets, but a two-step process including a low-temperature annealing (at 70 to 100 °C) and a high-temperature sintering step (around 180 °C) guaranteed the formation of continuous lines.

Figure 2g–i demonstrates the transformation of a soft material, amorphous Se (*a*-Se) nanoparticles, into continuous lines. In this case, a H_2SeO_3 solution in ethanol was spread on the polymer pattern, followed by exposure to N_2H_4 vapor to generate *a*-Se nanoparticles[14] (see Figure S4 in the Supporting Information). The randomly distributed *a*-Se nanoparticles were concentrated in the recessed regions upon heating at 90 °C for 30 min. The AFM image in Figure 2g shows that *a*-Se was separated from the polymer liquid and transformed into continuous solid lines. The phase image (Figure 2h) indicates that crystallization of PCL started from the interface at the Se lines during the cooling process. The secondary electron SEM image in Figure 2i shows parallel lines of Se and polymer.

The process could be extended to fabricate metal structures in other configurations. Figure 3 shows various

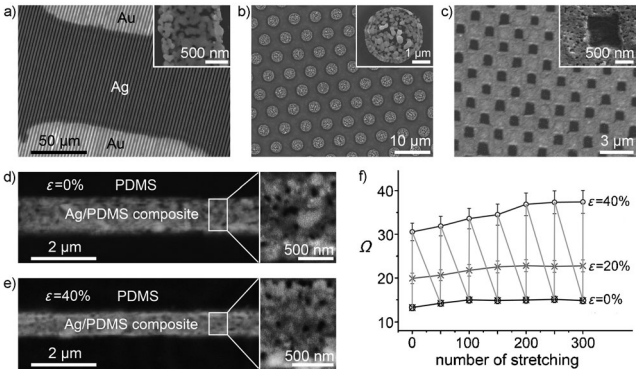

Figure 3. a–c) SEM images of Ag lines obtained from the Ag nanoparticles (30–50 nm in size) spread on different PCL patterns. The polymer layer was patterned into parallel lines across two Au electrodes on a Si wafer in (a), with an array of cylindrical holes on a PET substrate in (b), and as an array of square posts on a PET substrate in (c). d) SEM image of a conductive line consisting of Ag nanoparticles embedded in a PDMS matrix. e) SEM image of the composite line stretched at 40% uniaxial strain. The Ag nanoparticles maintained an interconnected network without mechanical failure. f) Change in electrical resistance (Ω) of a composite line during repeated cycles of stretching and relaxing. The resistance under strain (ε) was stabilized after a number of stretching/relaxing cycles.

examples of Ag structures obtained by the same precursor method. The patterns could be fabricated both on a rigid substrate and on a flexible polymer substrate because the CFL technique is applicable to any substrate. Figure 3a shows a SEM image of the Ag lines that were directly fabricated across two Au electrodes supported on a Si wafer. Because the initial sizes of the Ag nanoparticles were relatively large (30–50 nm), the re-organized nanoparticles formed porous but electrically conductive lines during the sintering procedure, as shown in the inset. The conductivity was comparable to that of bulk Ag (see Figure S5 in the Supporting Information). Figure 3b shows a SEM image of a 2D array of circular Ag disks obtained by using a PCL film with an array of cylindrical holes patterned on a poly(ethylene terephthalate) (PET) substrate. Figure 3c displays an Ag film with a 2D array of square holes. This Ag pattern was fabricated on a 2D array of PCL square pillars supported on a PET substrate. In this case, the precursor solution could spread and uniformly cover the entire surface of the polymer pattern, which was typically impossible to achieve with a flat PCL film. The topological barrier associated with the patterned PCL pillars seemed to support restricted collective dewetting of the precursor solution. The same approach has also been applied to other metals with relatively high melting

points (see Figure S6 in the Supporting Information), including Au, Cu, Fe, Co, and Ni. The precursors $AuCl_3$, $Cu(NO_3)_2$, $CoCl_2$, and $Ni(NO_3)_2$ were dissolved in ethanol at a concentration of 20 mM. After spreading the precursor solution on the PCL pattern, the precursor was reduced into metal by exposure to N_2H_4 vapor for 3 min. The samples were then annealed at 150 °C for 10 min, and PCL was dissolved in chloroform (see the Supporting Information for experimental details).

The porous structures of the Ag lines could be used to prepare polymer composites with an interpenetrating network (IPN) of conductive paths. A mixture of a polydimethylsiloxan (PDMS) monomer and its cross-linker (10:1, w/w) was poured onto the porous pattern of Ag lines prepared on a Si substrate, followed by thermal curing. When the cured PDMS was peeled off, the Ag lines were detached from the substrate and exposed to the air surface. Figure 3 d,e shows SEM images of the composite lines at zero strain ($\varepsilon = 0\,\%$) and at $\varepsilon = 40\,\%$ (apparent deformation of the PDMS support). As shown in the magnified images, the Ag nanoparticles remain in good contact in the IPN structure at 40 % of strain. Cracks were observed at $\varepsilon = 60\,\%$, which was mainly due to the PDMS tearing. The electrical properties also reflect this good stretchability. The lines of the Ag/PDMS composite have been previously demonstrated to be stretchable without losing conductivity.[15] Figure 3 f shows the changes in electrical resistance during repeated cycles of stretching and relaxing. The resistance was measured for a single composite line at two fixed positions separated by 500 μm before stretching. The resistance increased during stretching and returned to the original value after the strain was released. The increase of resistance with stretching can be ascribed to the increase in separation between the contact points and the reduction in the cross-sectional area. At a fixed strain, the resistance monotonically increased with the number of stretching/relaxing cycle and then reached a plateau value. The stabilization took roughly 150 cycles of stretching at $\varepsilon = 20\,\%$ and 250 cycles at $\varepsilon = 40\,\%$. Once stabilized at $\varepsilon = 40\,\%$, the resistance below $\varepsilon = 40\,\%$ showed good stability without any change during the stretching/relaxing cycles. This observation suggests that elongation of the elastomeric matrix probably forced the nanoparticles to rearrange their relative positions.

Soft materials separated from the polymer liquid and continuous solid lines without pores were generated. Figure 4 a shows a SEM image of parallel lines of In ($T_m = 156\,°C$) fabricated at 150 °C with $In(NO_3)_3$ as a precursor. Figure 4 b shows a SEM image of an array of hexagonal rings of Ga ($T_m = 29\,°C$). In this case, the solution of $Ga(NO_3)_3$ was spread on a PCL film with an array of hexagonal holes and then reduced by N_2H_4 vapor, followed by thermal annealing at 150 °C. The polymer pattern has a residual layer (150 nm) in the recessed hexagonal region (see Figure S7 in the Supporting Information). Upon annealing the polymer liquid flowed to the edge region of each hexagon from both outside and inside of the hexagon, generating a hexagonal ring of Ga. When there was no residual layer in the recessed region, the metal was collected in the center of each recessed region and generated a disk. Figure 4 c shows a SEM image of a chessboard pattern of In fabricated on a PCL film patterned with an array of square holes that have no residual polymer layer.

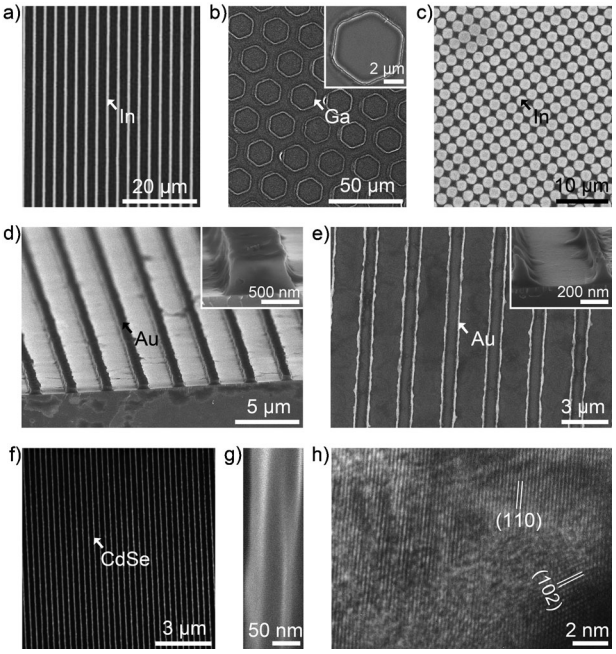

Figure 4. a–c) Structures of soft materials obtained from their nanoparticles deposited on different PCL patterns supported on Si substrates. Solutions of precursors of In and Ga were spread on the polymer patterns and then reduced by exposure to N_2H_4 vapor. The polymer layer was patterned into an array of parallel lines in (a), with an array of hexagonal holes and a residual layer in each hole in (b), and with an array of square holes with no residual layer in the hole in (c). d,e) Parallel lines of Au fabricated with pre-synthesized Au nanoparticles (8 nm) scattered on a PCL pattern. Depending on the concentration of the Au nanoparticles, single or dual lines were generated. The insets are magnified images of the lines. f–h) Parallel lines (single) of CdSe generated from pre-synthesized CdSe quantum dots (4 nm) spread on a PCL pattern. The lines were continuous (g) and the crystal grains were larger than the original quantum dots (h).

The melting points of the nanoparticles are dramatically reduced when their sizes are below 10 nm.[16] The use of uniform pre-made nanoparticles facilitates a close packing of the nanoparticles and enables the fine-tuning of the phase separation from the patterned polymer. As such, the production of fine features without pores, resembling those obtained from materials with low melting points, is possible. Figure 4 d–h shows parallel lines patterned with Au (d,e) and CdSe nanoparticles (f–h). The synthetic procedure was essentially the same as that for the samples shown in Figures 1 and 2 except for the use of pre-synthesized Au (8 ± 3) nm and CdSe (4 ± 2) nm nanoparticles (see Figure S8 in the Supporting Information) as starting materials. The Au nanoparticles were passivated by tetrachloro-*o*-benzoquinone[17] and the CdSe nanoparticles were covered by hydroxyl groups.[18] After spreading the nanoparticles on a PCL pattern, the sample was annealed at 200 °C for 60 min under N_2. Figure 4 d shows a cross-sectional SEM image of the solid lines of Au, which had well-defined dimensions (500 nm thick and 700 nm wide). When a less concentrated suspension of Au nanoparticles was

used, most of the nanoparticles were selectively deposited at the bottom edges of the PCL lines. Thermal annealing transformed the nanoparticles into two continuous, thin solid lines (Figure 4e). The inset shows a cross-sectional image of the dual Au lines with a width of 120 nm. Similar dual lines were also observed in the patterning of Ga (see Figure S9 in the Supporting Information) when a small amount of Ga precursor was used. In contrast, we obtained narrow, single lines of CdSe quantum dots regardless of the particle concentration on the same PCL line pattern. This pattern is due to the stronger phase separation between the hydrophilic quantum dots and the polymer as well as a better affinity of the quantum dots towards the substrate. The optical micrograph in Figure 4f clearly showes continuity and good uniformity of the CdSe lines. Figure 4g shows a magnified SEM image of one CdSe line, which was roughly 80 nm in width. The thinnest lines we have fabricated were about 50 nm which is the lower limit for inorganic materials. Thinner lines tended to break into dots because of the Rayleigh instability on an incompatible surface (see Figure S10 in the Supporting Information). The high-resolution TEM image in Figure 4h shows that the CdSe quantum dots sintered together and generated multigrained lines. The upper limit of the pattern size was roughly around 30 μm because the fluid of the patterned polymer did not concentrate all the materials in the trenched region.

In summary, we have demonstrated a simple technique that can be used to directly pattern inorganic materials. For this technique, the material to be patterned was randomly deposited on the surface of a patterned crystalline polymer. Upon heating, the viscoelastic polymer liquid flowed to the recessed area and the materials separating from the polymer melt assembled into continuous structures in the recessed regions. Hard materials generated continuous, porous structures which could be used to generate stretchable, conductive electrodes. Soft materials evolved into continuous, solid structures with a sharp interface to the polymer melt. This new technique can be extended to fabricate flexible or stretchable circuits because of its compatibility to polymer substrates.

Received: June 21, 2011
Revised: September 9, 2011
Published online: September 26, 2011

Keywords: nanoparticles · phase separation · self-organization · soft lithography · viscoelastic flow

[1] Y. Xia, J. A. Rogers, K. E. Paul, G. M. Whitesides, *Chem. Rev.* **1999**, *99*, 1823 – 1848.
[2] S. Y. Chou, P. R. Krauss, P. J. Renstrom, *Science* **1996**, *272*, 85 – 87.
[3] K. Y. Suh, Y. S. Kim, H. H. Lee, *Adv. Mater.* **2001**, *13*, 1386 – 1389.
[4] Y. S. Kim, K. Y. Suh, H. H. Lee, *Appl. Phys. Lett.* **2001**, *79*, 2285 – 2287.
[5] S. Jeon, E. Menard, J.-U. Park, J. Maria, M. Meitl, J. Zaumseil, J. A. Rogers, *Adv. Mater.* **2004**, *16*, 1369 – 1373.
[6] J. A. Rogers, R. G. Nuzzo, *Mater. Today* **2005**, *8*, 50 – 56.
[7] P. Yang, G. Wirnsberger, H. C. Huang, S. R. Cordero, M. D. McGehee, B. Scott, T. Deng, G. M. Whitesides, B. F. Chmelka, S. K. Buratto, G. D. Stucky, *Science* **2000**, *287*, 465 – 467.
[8] P. Yang, A. H. Rizvi, B. Messer, B. F. Chmelka, G. M. Whitesides, G. D. Stucky, *Adv. Mater.* **2001**, *13*, 427 – 431.
[9] C. M. Bruinink, M. Péter, P. A. Maury, M. de Boer, L. Kuipers, J. Huskens, D. N. Reinhoudt, *Adv. Funct. Mater.* **2006**, *16*, 1555 – 1565.
[10] I. Korczagin, S. Golze, M. A. Hempenius, G. J. Vancso, *Chem. Mater.* **2003**, *15*, 3663 – 3668.
[11] J. C. Love, K. E. Paul, G. M. Whitesides, *Adv. Mater.* **2001**, *13*, 604 – 607.
[12] B. D. Gates, Q. Xu, V. R. Thalladi, T. Cao, T. Knickerbocker, G. M. Whitesides, *Angew. Chem.* **2004**, *116*, 2840 – 2843; *Angew. Chem. Int. Ed.* **2004**, *43*, 2780 – 2783.
[13] H. E. Jeong, S. H. Lee, P. Kim, K. Y. Suh, *Nano Lett.* **2006**, *6*, 1508 – 1513.
[14] U. Jeong, Y. Xia, *Adv. Mater.* **2005**, *17*, 102 – 106.
[15] D. C. Hyun, M. Park, C. Park, B. Kim, Y. Xia, J. H. Hur, J. J. Park, U. Jeong, *Adv. Mater.* **2011**, DOI: 10.1002/adma.201100639.
[16] F. Ercolessi, W. Andreoni, E. Tosatti, *Phys. Rev. Lett.* **1991**, *66*, 911 – 914.
[17] D. G. Duff, A. Baiker, P. P. Edwards, *Langmuir* **1993**, *9*, 2301 – 2309.
[18] T.-L. Wang, C.-H. Yang, Y.-T. Shieh, A.-C. Yeh, *Macromol. Rapid Commun.* **2009**, *30*, 1679 – 1683.

